

1 R-Z Geometry

Solving the transport equation in different coordinate systems may provide simpler ways of modeling a particular geometry or symmetry. In this section, we derive the *R-Z* transport equation to be solved. It assumes there is no variation in the azimuthal direction (of a cylinder), hence problems in *R-Z* geometry look very similar to problems in *X-Y* geometry. The streaming operator in cylindrical geometry is [?]

$$\boldsymbol{\Omega} \cdot \nabla \psi = \frac{\mu}{r} \frac{\partial}{\partial r}(r\psi) + \frac{\eta}{r} \frac{\partial \psi}{\partial \zeta} + \xi \frac{\partial \psi}{\partial z} - \frac{1}{r} \frac{\partial}{\partial \omega}(\eta\psi), \quad (1)$$

where $\boldsymbol{\Omega}$ is the direction of travel unit vector, ψ is the angular flux, and

$$\mu \equiv \boldsymbol{\Omega} \cdot \hat{e}_r = \sqrt{1 - \xi^2} \cos \omega = \sin(\theta) \cos(\omega), \quad (2)$$

$$\eta \equiv \boldsymbol{\Omega} \cdot \hat{e}_\theta = \sqrt{1 - \xi^2} \sin \omega = \sin(\theta) \sin(\omega), \quad (3)$$

$$\xi \equiv \boldsymbol{\Omega} \cdot \hat{e}_z = \cos(\theta). \quad (4)$$

The variables μ , η , ξ , ω , and θ are shown in the cylindrical coordinate system in Figure 1. We assume there is no solution variation in the azimuthal direction, i.e.

$$\frac{\partial \psi}{\partial \zeta} \equiv 0, \quad (5)$$

which simplifies the streaming term to

$$\boldsymbol{\Omega} \cdot \nabla \psi = \frac{\mu}{r} \frac{\partial}{\partial r}(r\psi) + \xi \frac{\partial \psi}{\partial z} - \frac{1}{r} \frac{\partial}{\partial \omega}(\eta\psi). \quad (6)$$

The transport equation in *R-Z* geometry is then

$$\begin{aligned} \frac{\mu}{r} \frac{\partial}{\partial r} r\psi(r, z, \boldsymbol{\Omega}) + \xi \frac{\partial}{\partial z} \psi(r, z, \boldsymbol{\Omega}) - \frac{1}{r} \frac{\partial}{\partial \omega} \eta\psi(r, z, \boldsymbol{\Omega}) + \sigma_t(r, z) \psi(r, z, \boldsymbol{\Omega}) \\ = \frac{1}{4\pi} \int_{4\pi} \sigma_s(r, z) I(r, z, \boldsymbol{\Omega}') d\Omega' + S_0(r, z, \boldsymbol{\Omega}) \end{aligned} \quad (7)$$

where σ_t is the total cross section, σ_s is the scattering cross section, and S_0 is an isotropic source as before.

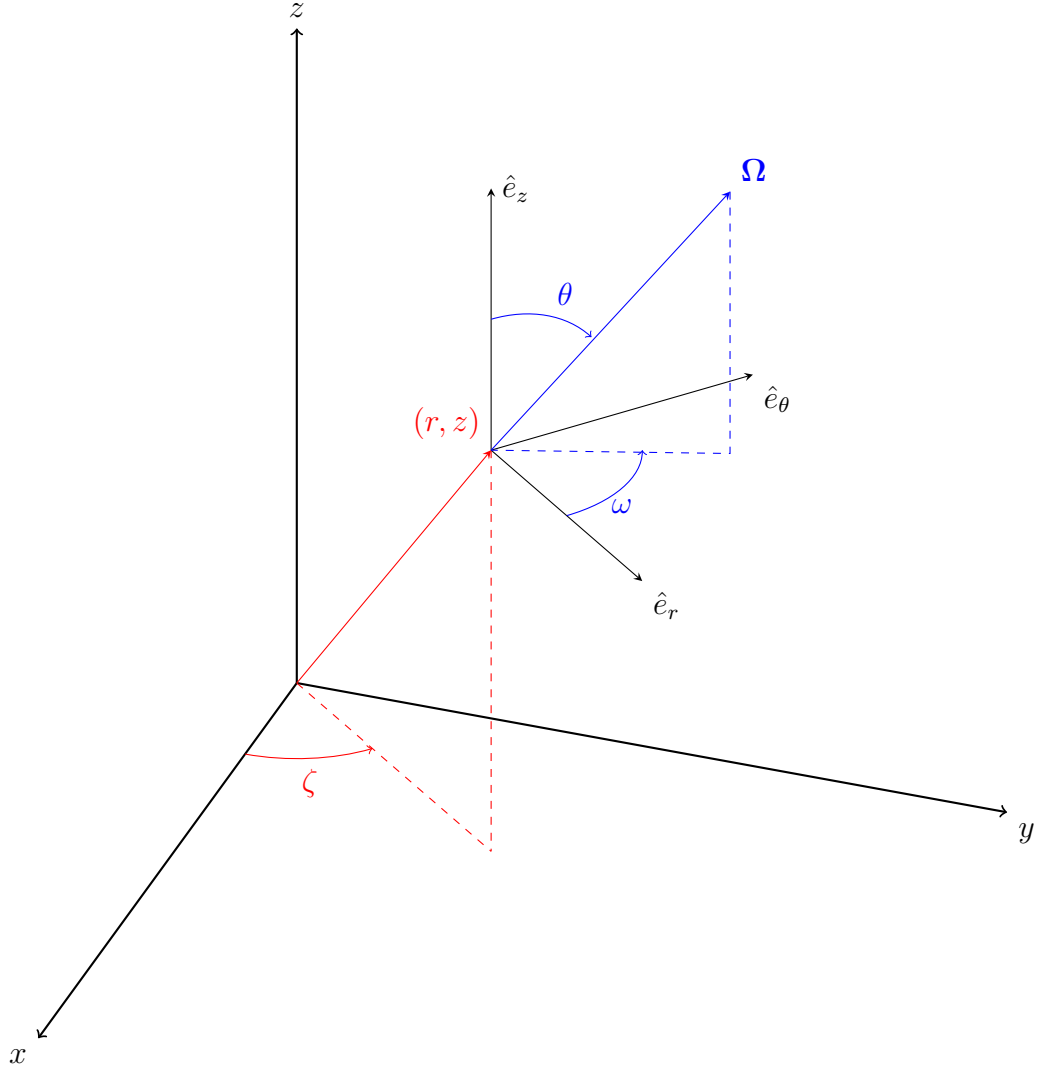


Figure 1: Cylindrical space-angle coordinate system showing the position (r, z) and direction of travel Ω .

1.1 Angular Discretization

Discretizing Equation 7 with a level-symmetric angular quadrature results in

$$\begin{aligned} \frac{\mu_{n,m}}{r} \frac{\partial}{\partial r} r \psi_{n,m}(r, z) + \xi_n \frac{\partial}{\partial z} \psi_{n,m}(r, z) - \frac{1}{r} \frac{\partial}{\partial \omega} \eta_{n,m} \psi_{n,m}(r, z) + \sigma_t(r, z) \psi_{n,m}(r, z) \\ = \frac{1}{4\pi} \int_{4\pi} \sigma_s(r, z) I(r, z, \Omega') d\Omega' + S_0(r, z, \Omega) \quad (8) \end{aligned}$$

for direction $\Omega_{n,m}$, where index \$n\$ describes a level of quadrature with constant \$\xi\$ and

the m index denotes the quadrature point on that level. The (n, m) indexing is shown in Figure 2.

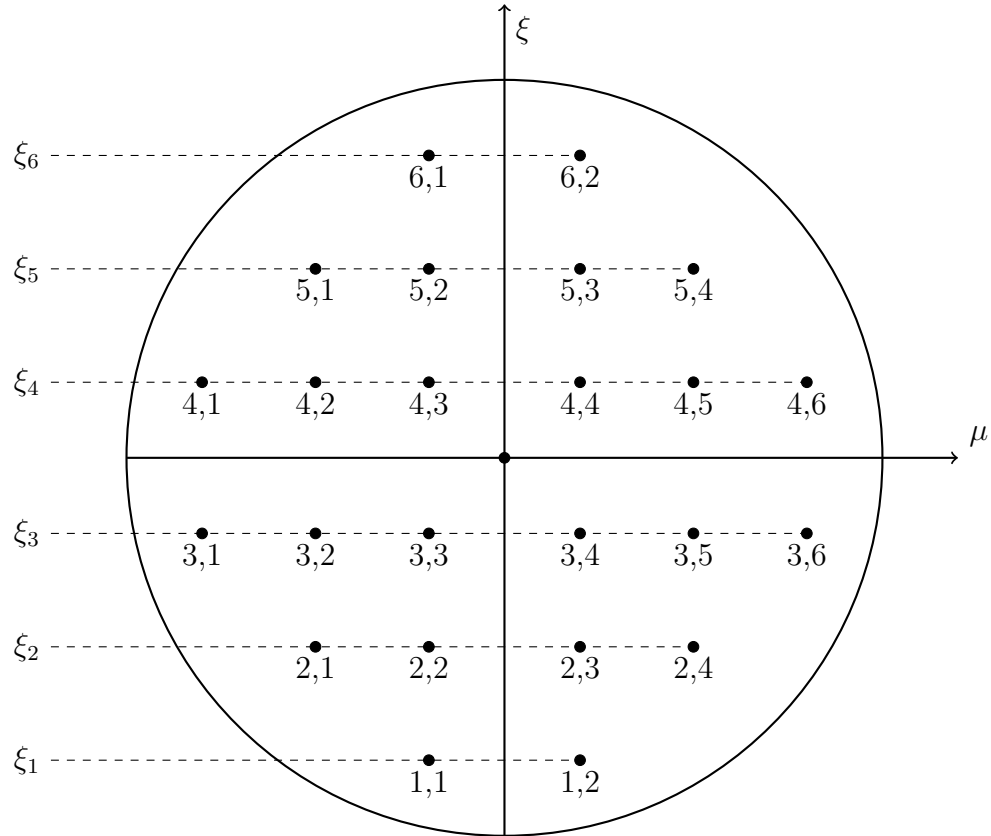


Figure 2: Angular discretization showing (ξ, μ) pairs; adapted from [?]

One of the major challenges is handling the angular derivative term. Lewis and Miller [?] describes an approximation for the partial derivative of the intensity with respect to ω :

$$-\frac{1}{r} \frac{\partial}{\partial \omega} \eta_{m,n} \psi_{n,m}(r, z) = \frac{\alpha_{m+1/2}^n \psi_{n,m+1/2}(r, z) - \alpha_{m-1/2}^n \psi_{n,m-1/2}(r, z)}{rw_{n,m}} \quad (9)$$

where $\alpha_{m+1/2}^n$ and $\alpha_{m-1/2}^n$ are angular differencing coefficients, and $w_{n,m}$ is the angular

quadrature weight. We substitute this into Equation 18,

$$\begin{aligned} & \frac{\mu_{n,m}}{r} \frac{\partial}{\partial r} r \psi_{n,m}(r, z) + \xi_n \frac{\partial}{\partial z} \psi_{n,m}(r, z) \\ & + \frac{\alpha_{m+1/2}^n \psi_{m+1/2,n}(r, z) - \alpha_{m-1/2}^n \psi_{m-1/2,n}(r, z)}{rw_{n,m}} + \sigma_t(r, z) \psi_{n,m}(r, z) \\ & = \frac{1}{4\pi} \int_{4\pi} \sigma_s(r, z) \psi(r, z, \Omega') d\Omega' + \frac{1}{4\pi} S_0(r, z) \quad (10) \end{aligned}$$

Here, we pause to notice that there are similarities and differences between our Cartesian discretization. The absorption term, axial derivative term, and right-hand-side are the same in both coordinate systems. The differences arise in the radial and angular derivative terms.

After multiplying through by the radius r , the radial derivative term has a factor of r inside the derivative. The angular derivative term is also new and does not resemble a mass matrix so MFEM will require additional modification.

Requiring Equation 10 to satisfy the uniform infinite medium solution results in the condition,

$$\alpha_{m+1/2}^n = \alpha_{m-1/2}^n - \mu_{n,m} w_{n,m} \quad (11)$$

If $\alpha_{1/2}^n$ is known, then the remaining coefficients are uniquely determined. To find $\alpha_{1/2}^n$, we require that Equation 10 satisfy the conservation equation (Eq. 7). Given a quadrature set with an even number of $\mu_{n,m}$ values, setting $\alpha_{1/2}^n = 0$ results in $\alpha_{M_n+1/2}^n = 0$ per Equation 11 and the conservation equation is satisfied.

A relationship between $\psi_{n,m}$, $\psi_{n,m+1/2}$, and $\psi_{n,m-1/2}$ must be established. A weighted diamond difference scheme has been established by Morel and Montry [?],

$$\psi_{n,m}(r, z) = \tau_{n,m} \psi_{n,m+1/2} + (1 - \tau_{n,m}) \psi_{n,m-1/2} \quad (12)$$

where $\tau_{n,m}$ linearly interpolates μ :

$$\tau_{n,m} = \frac{\mu_{n,m} - \mu_{n,m-1/2}}{\mu_{n,m+1/2} - \mu_{n,m-1/2}} \quad (13)$$

with

$$\mu_{n,m+1/2} = \sqrt{1 - \xi_n^2} \cos(\varphi_{n,m+1/2}) \quad (14)$$

$$\varphi_{n,m+1/2} = \varphi_{n,m-1/2} + \pi \frac{w_{n,m}}{w_n} \quad (15)$$

$$w_n = \sum_{m=1}^{M_n} w_{n,m} \quad (16)$$

We take Equation 10, multiply through by r and perform a product rule on the radial derivative term,

$$\begin{aligned} & \mu_{n,m} \left[\psi_{n,m}(r, z) + r \frac{\partial}{\partial r} \psi_{n,m}(r, z) \right] + r \xi_n \frac{\partial}{\partial z} \psi_{n,m}(r, z) \\ & + \frac{\alpha_{m+1/2}^n \psi_{m+1/2,n}(r, z) - \alpha_{m-1/2}^n \psi_{m-1/2,n}(r, z)}{w_{n,m}} + r \sigma_t(r, z) \psi_{n,m}(r, z) \\ & = \frac{r}{4\pi} \int_{4\pi} \sigma_s(r, z) \psi(r, z, \Omega') d\Omega' + \frac{r}{4\pi} S_0(r, z). \end{aligned} \quad (17)$$

We solve Equation 12 for $\psi_{n,m+1/2}$, perform a substitution, and move the known quantities to the right-hand-side,

$$\begin{aligned} & \mu_{n,m} r \frac{\partial}{\partial r} \psi_{n,m}(r, z) + r \xi_n \frac{\partial}{\partial z} \psi_{n,m}(r, z) + \mu_{n,m} \psi_{n,m}(r, z) \\ & + \frac{\alpha_{m+1/2}^n}{\tau_{n,m} w_{n,m}} \psi_{n,m}(r, z) + r \sigma_t(r, z) \psi_{n,m}(r, z) \\ & = \frac{r}{4\pi} \int_{4\pi} \sigma_s(r, z) \psi(r, z, \Omega') d\Omega' + \frac{r}{4\pi} S_0(r, z) \\ & + \left(\frac{1 - \tau_{n,m}}{\tau_{n,m}} \frac{\alpha_{m+1/2}^n}{w_{n,m}} + \frac{\alpha_{m-1/2}^n}{w_{n,m}} \right) \psi_{n,m-1/2}(r, z). \end{aligned} \quad (18)$$

Given a level-symmetric quadrature set, all of the $\alpha_{n,m\pm 1/2}^n$ and $\tau_{n,m}$ values can be computed. We solve the starting direction equation to obtain $\psi_{n,1/2}$. That is, we

solve the X - Y system for directions $\Omega_{n,1/2}$,

$$\Omega_{n,1/2} \cdot \nabla \psi_{n,1/2} + \sigma_t \psi_{n,1/2} = \frac{1}{4\pi} \sigma_s \phi + \frac{1}{4\pi} S_0 \quad (19)$$

There is an alternate angular discretization method developed by Warsa and Prinja [?]. Instead of finding an approximation for the angular derivative, they perform a product rule:

$$\frac{\partial \psi}{\partial \omega} \equiv \frac{\partial \mu}{\partial \omega} \frac{\partial \psi}{\partial \mu} \quad (20)$$

Since,

$$\frac{\partial \mu}{\partial \omega} \equiv -\xi, \quad (21)$$

The angular derivative can be written

$$\frac{\partial \psi}{\partial \omega} \equiv -\xi \frac{\partial \psi}{\partial \mu} \quad (22)$$

Here, an approximation for the μ -derivative must be established.

1.2 Spatial Discretization

The finite element discretization is performed here. The methodology is similar to the Cartesian geometry. First, we subdivide a problem domain using a spatial mesh. Then, we multiply Equation 18 by a test function and integrate over the volume of a single mesh zone,

$$\begin{aligned} & (r \Omega_{n,m} \cdot \nabla \psi_{n,m}, v_i)_{\mathbb{D}} + (\mu_{n,m} \psi_{n,m}, v_i)_{\mathbb{D}} \\ & + \left(\frac{\alpha_{m+1/2}^n}{\tau_{n,m} w_{n,m}} \psi_{n,m}, v_i \right)_{\mathbb{D}} + (r \sigma_t \psi_{n,m}, v_i)_{\mathbb{D}} \\ & = \left(\frac{r}{4\pi} \int_{4\pi} \sigma_s \psi d\Omega', v_i \right)_{\mathbb{D}} + \left(\frac{r}{4\pi} S_0, v_i \right)_{\mathbb{D}} \\ & + \left(\left(\frac{1 - \tau_{n,m}}{\tau_{n,m}} \frac{\alpha_{m+1/2}^n}{w_{n,m}} + \frac{\alpha_{m-1/2}^n}{w_{n,m}} \right) \psi_{n,m-1/2}, v_i \right)_{\mathbb{D}}, \end{aligned} \quad (23)$$

where the Cartesian gradient operator is used and the inner product notation,

$$(a, b)_{\mathbb{D}} \equiv \int_{\mathbb{D}} ab, \quad (24)$$

is used. We perform an integration by parts,

$$\begin{aligned} & (r\boldsymbol{\Omega}_{n,m} \cdot \hat{n}\psi_{n,m}, v_i)_{\partial\mathbb{D}} - (r\psi_{n,m}, \boldsymbol{\Omega}_{n,m} \cdot \nabla v_i)_{\mathbb{D}} + (\mu_{n,m}\psi_{n,m}, v_i)_{\mathbb{D}} \\ & + \left(\frac{\alpha_{m+1/2}^n}{\tau_{n,m}w_{n,m}} \psi_{n,m}, v_i \right)_{\mathbb{D}} + (r\sigma_t\psi_{n,m}, v_i)_{\mathbb{D}} \\ & = \left(\frac{r}{4\pi} \int_{4\pi} \sigma_s \psi d\Omega', v_i \right)_{\mathbb{D}} + \left(\frac{r}{4\pi} S_0, v_i \right)_{\mathbb{D}} \\ & + \left(\left(\frac{1 - \tau_{n,m}}{\tau_{n,m}} \frac{\alpha_{m+1/2}^n}{w_{n,m}} + \frac{\alpha_{m-1/2}^n}{w_{n,m}} \right) \psi_{n,m-1/2}, v_i \right)_{\mathbb{D}}, \end{aligned} \quad (25)$$

to obtain our angular and spatially discretized R - Z transport equation.

WE PERFORMED SOME STUDIES TO MAKE SURE IT'S RIGHT...

We first solved a uniform infinite medium problem with $\sigma_t = 1.0$, $\sigma_s = 0.3$, and $S_0 = 0.7$ for 1st-order FEM on a 2nd-order mesh using S_4 level-symmetric angular quadrature. The solution, shown in Figure 3, demonstrates we get the exact flat solution of $\phi = 1.0$.

We tested several MMS problems as well. First, we defined the manufactured solution

$$\psi = (1 - \mu^2)(1 - \xi^2) \sin\left(\frac{\pi}{2}r\right) \cos(\pi z) \quad (26)$$

with 2nd-order FEM, Orthogonal quadrilateral mesh, $\sigma_t = 1.0$, $\sigma_s = 0.3$, $S_0 = 0.7$, S_4 level-symmetric angular quadrature. The solution is shown in Figure 4 and the L²-error was 0.132.

Removing the angular dependence in the manufactured solution,

$$\psi = \sin\left(\frac{\pi}{2}r\right) \cos(\pi z), \quad (27)$$

increased the accuracy of our DGFEM approximation. Shown in Figure 5, the L²-

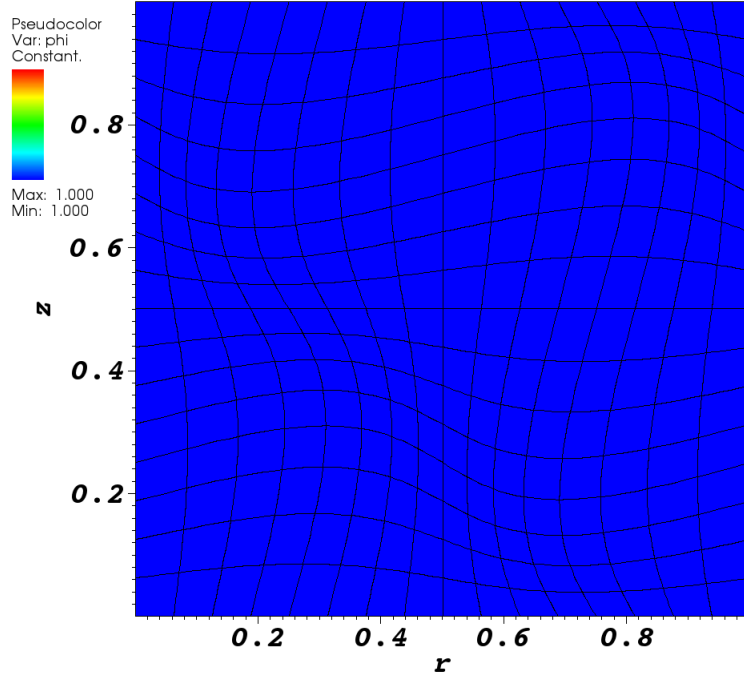


Figure 3: Uniform infinite medium solution.

error was reduced to 4.59×10^{-5} .

Bailey et al. [?] showed 2nd-order convergence using PWLD and BLD using the manufactured solution

$$\psi_{\text{MMS}}(r, z) = (\sin(\pi r) + 1 - r) \sin(\pi z), \quad (28)$$

for $\sigma_t = 3 \text{ cm}^{-1}$ and $\sigma_s = 0.9999\sigma_t$. We solved this same problem using $p = \{1, 2, 4, 6, 8\}$ on an orthogonal and 2nd-order curved mesh using S_8 level-symmetric angular quadrature. The incident angular flux is equal to Equation 28. Figure 6 shows the $p = 2$ solution on a 2nd-order mesh.

The spatial convergence study performed by Bailey et al. demonstrated 2nd-order converge for their 1st-order methods. Figures 7a and 7b demonstrate $O(p+1)$ convergence on an orthogonal mesh and 2nd-order mesh, respectively. Reference lines

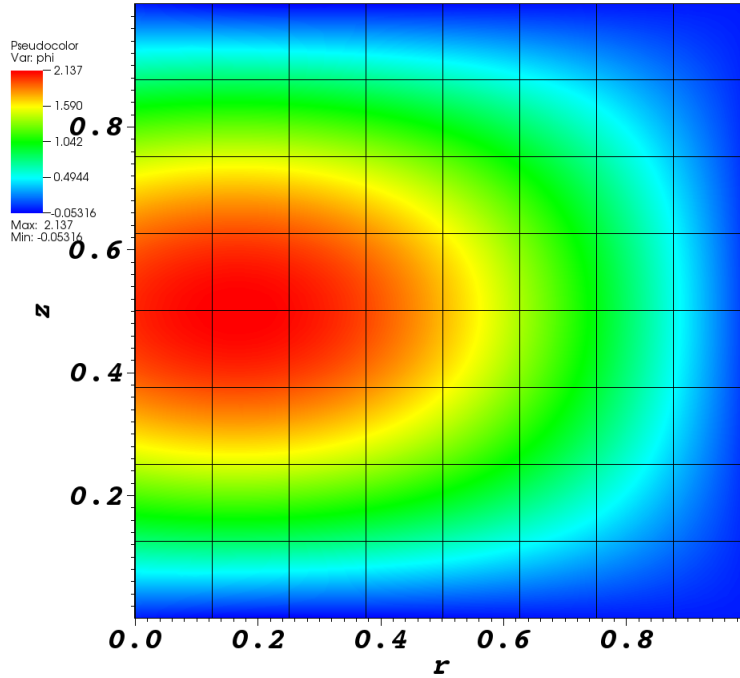


Figure 4: MMS solution for Equation 26.

are also provided for comparison.

1.3 Lumping

1.4 Diffusion Synthetic Acceleration

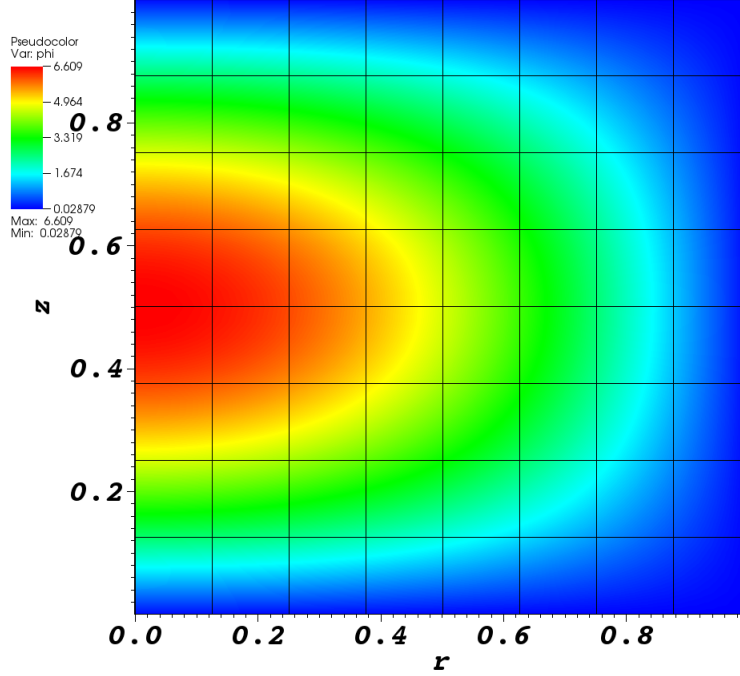


Figure 5: MMS solution for Equation 27.

1.5 Symmetry Preservation

We want R - Z geometry to solve and preserve 1-dimensional spherical solutions. The transport equation in spherical geometry is

$$\Omega \cdot \nabla \psi = \frac{\partial \psi}{\partial r} \Omega \cdot \nabla r + \frac{\partial \psi}{\partial \mu} \Omega \cdot \nabla \mu \quad (29)$$

$$= \mu \frac{\partial \psi}{\partial r} + \frac{(1 - \mu^2)}{r} \frac{\partial \psi}{\partial \mu} \quad (30)$$

$$= \frac{\mu}{r^2} \frac{\partial}{\partial r} (r^2 \psi) + \frac{\partial}{\partial \mu} \left[\frac{(1 - \mu^2) \psi}{r} \right] \quad (31)$$

$$\mu \frac{\partial}{\partial r} (r^2 \psi) + r \frac{\partial}{\partial \mu} ((1 - \mu^2) \psi) + r^2 \sigma_t \psi = \frac{1}{4\pi} \sigma_s \phi + \frac{1}{4\pi} S_0. \quad (32)$$

In 1-dimensional geometry, this simplifies to

$$\mu \frac{\partial \psi}{\partial r} + \sigma_t \psi = \frac{1}{4\pi} \sigma_s \phi + \frac{1}{4\pi} S_0. \quad (33)$$

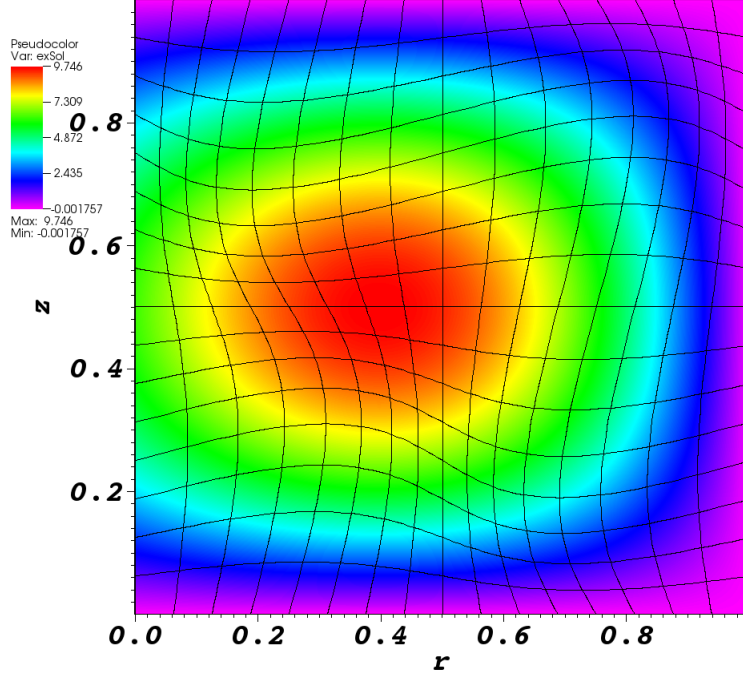


Figure 6: MMS solution to Equation 28.

We can solve this for ψ .

$$\frac{\partial \psi(r)}{\partial r} e^{\sigma_t r / \mu} + \frac{\sigma_t}{\mu} \psi(r) e^{\sigma_t r / \mu} = \frac{1}{4\pi\mu} (\sigma_s \phi + S_0) e^{\sigma_t r / \mu} \quad (34)$$

$$\frac{\partial}{\partial r} (\psi(r) e^{\sigma_t r / \mu}) = \frac{1}{4\pi\mu} (\sigma_s \phi + S_0) e^{\sigma_t r / \mu} \quad (35)$$

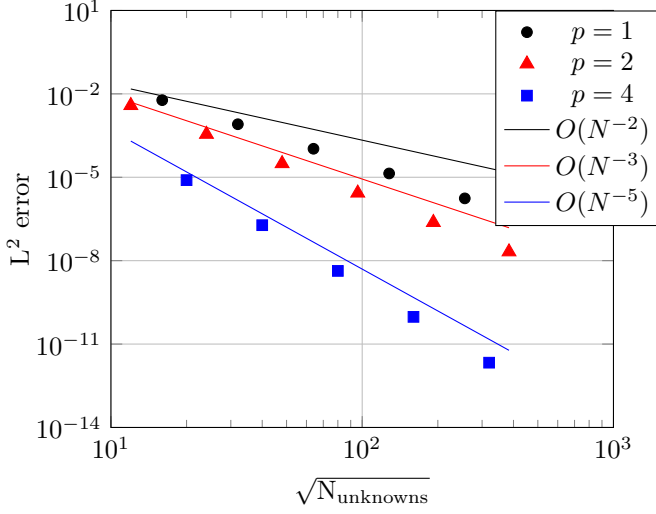
$$\int \frac{\partial}{\partial r'} (\psi(r') e^{\sigma_t r' / \mu}) dr' = \frac{1}{4\pi\mu} \int (\sigma_s \phi(r') + S_0) e^{\sigma_t r' / \mu} dr' \quad (36)$$

$$\psi(r) e^{\sigma_t r / \mu} - c = \frac{1}{4\pi\mu} \int (\sigma_s \phi(r') + S_0) e^{\sigma_t r' / \mu} dr' \quad (37)$$

$$\psi(r) = e^{-\sigma_t r / \mu} \frac{1}{4\pi\mu} \int (\sigma_s \phi(r') + S_0) e^{\sigma_t r' / \mu} dr' + ce^{-\sigma_t r / \mu} \quad (38)$$

$$\psi(1) = 1 = e^{-\sigma_t / \mu} \frac{1}{4\pi\mu} \int (\sigma_s \phi(r') + S_0) e^{\sigma_t r' / \mu} dr' + ce^{-\sigma_t / \mu} \quad (39)$$

$$c = e^{\sigma_t / \mu} - \frac{1}{4\pi\mu} \int (\sigma_s \phi(r') + S_0) e^{\sigma_t r' / \mu} dr' \quad (40)$$



(a) Orthogonal quadrilateral mesh.

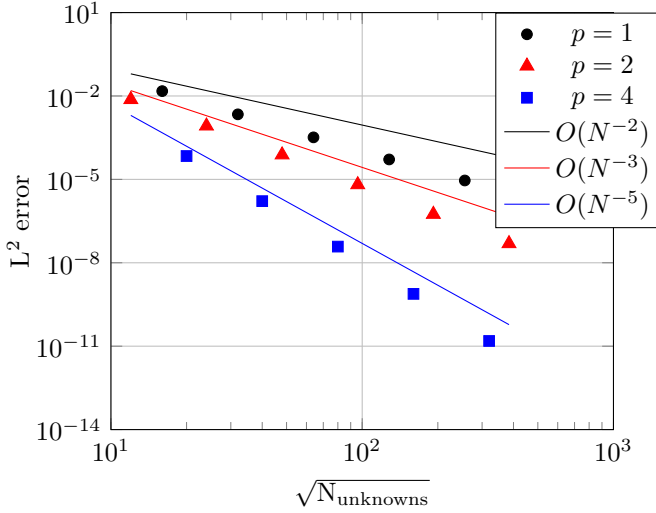
(b) 2nd-order curved mesh.

Figure 7: L^2 -norm of the errors from the manufactured solution and reference lines, where $N_{\text{unknowns}} = N_{\text{cells}}(p + 1)^2$.

$$\begin{aligned} \psi(r) = e^{-\sigma_t r / \mu} \frac{1}{4\pi\mu} \int (\sigma_s \phi(r') + S_0) e^{\sigma_t r' / \mu} dr' + \\ \left[e^{\sigma_t / \mu} - \frac{1}{4\pi\mu} \int (\sigma_s \phi(r') + S_0) e^{\sigma_t r' / \mu} dr' \right] e^{-\sigma_t r / \mu} \quad (41) \end{aligned}$$

$$\psi(r) = e^{-\sigma_t r / \mu} \frac{1}{4\pi\mu} \int (\sigma_s \phi(r') + S_0) e^{\sigma_t r' / \mu} dr' + e^{(1-r)\sigma_t / \mu} - e^{-\sigma_t r / \mu} \frac{1}{4\pi\mu} \int (\sigma_s \phi(r') + S_0) e^{\sigma_t r' / \mu} dr' \quad (42)$$

$$\psi(r) = e^{(1-r)\sigma_t / \mu} \quad (43)$$

We use MMS to solve a 1-D spherical problem using the *R-Z* geometry spatial discretization. The manufactured solution is

$$\psi_{\text{MMS}}(\rho) = \sin(\pi\rho) + 2 - \rho, \quad (44)$$

where $\rho = \sqrt{r^2 + z^2}$ is the distance from the origin (i.e. the spherical radius). First, we integrate the streaming term by parts,

$$\boldsymbol{\Omega} \cdot \nabla \psi = \mu \frac{\partial \psi}{\partial r} + \frac{\mu}{r} \psi + \xi \frac{\partial \psi}{\partial r} - \frac{\mu}{r} \psi - \frac{\eta}{r} \frac{\partial \psi}{\partial \omega} \quad (45)$$

$$= \mu \frac{\partial \psi}{\partial r} + \xi \frac{\partial \psi}{\partial z} - \frac{\eta}{r} \frac{\partial \psi}{\partial \omega} \quad (46)$$

Substituting the manufactured solution into this *R-Z* transport equation,

$$\begin{aligned} & \mu \frac{\partial}{\partial r} (\sin(\pi\rho) + 2 - \rho) + \xi \frac{\partial}{\partial z} (\sin(\pi\rho) + 2 - \rho) \\ & - \frac{\eta}{r} \frac{\partial}{\partial \omega} [(\sin(\pi\rho) + 2 - \rho)] + \sigma_t (\sin(\pi\rho) + 2 - \rho) \\ & = \frac{1}{2\pi} \sigma_s \phi_{\text{MMS}} + \frac{1}{2\pi} S_0. \end{aligned} \quad (47)$$

Integrating ψ_{MMS} over all directions reveals ϕ_{MMS} ,

$$\begin{aligned} & \mu \frac{\partial}{\partial r} (\sin(\pi\rho) + 2 - \rho) + \xi \frac{\partial}{\partial z} (\sin(\pi\rho) + 2 - \rho) \\ & - \frac{\eta}{r} \frac{\partial}{\partial \omega} [(\sin(\pi\rho) + 2 - \rho)] + \sigma_t (\sin(\pi\rho) + 2 - \rho) \\ & = \sigma_s (\sin(\pi\rho) + 2 - \rho) + \frac{1}{2\pi} S_0. \end{aligned} \quad (48)$$

We perform some simplifications,

$$\frac{\partial \psi}{\partial r} = \frac{\pi r \cos(\pi \sqrt{r^2 + z^2})}{\sqrt{r^2 + z^2}} - \frac{r}{\sqrt{r^2 + z^2}} \quad (49)$$

$$\frac{\partial \psi}{\partial z} = \frac{\pi z \cos(\pi \sqrt{r^2 + z^2})}{\sqrt{r^2 + z^2}} - \frac{r}{\sqrt{r^2 + z^2}} \quad (50)$$

$$\begin{aligned} & \mu \frac{\partial}{\partial r} (\sin(\pi\rho) + 2 - \rho) + \xi \frac{\partial}{\partial z} (\sin(\pi\rho) + 2 - \rho) \\ & - \frac{\eta}{r} \frac{\partial}{\partial \omega} [(\sin(\pi\rho) + 2 - \rho)] + \sigma_t (\sin(\pi\rho) + 2 - \rho) \\ & = \sigma_s (\sin(\pi\rho) + 2 - \rho) + \frac{1}{2\pi} S_0. \end{aligned} \quad (51)$$

Because of the angular derivative in the streaming term, we reduce the influence of the direction dependence as much as possible by using higher order level-symmetric angular quadrature.

We evaluate the relative asymmetry by calculating the averages of all nodes at each ρ value and

$$\phi_{\text{sym}}(\rho, \theta) = \frac{\phi_{\text{code}}(\rho, \theta) - \phi_{\text{avg}}(\rho)}{\phi_{\text{avg}}(\rho)}, \quad (52)$$

where

$$\phi_{\text{avg}}(\rho) = \frac{1}{N_{\text{nodes}}(\rho)} \sum_{i=1}^{N_{\text{nodes}}(\rho)} \phi(\rho, \theta_i) \quad (53)$$

is the average scalar flux at all nodes at the same spherical radius ρ .

1.5.1 Linear in Spherical Radius

The three traditional coordinate systems are Cartesian, cylindrical, and spherical. It is straight forward to describe a spatial position using any one of them. However, challenges arise when spatially discretizing. Specifically, angular derivatives arise inside

the streaming term in cylindrical and spherical geometries. In modeling a spherical problem, it would seem best to use a spherical coordinate system to describe the spatial domain. However, there are two angular derivatives that must now be handled with a numerical scheme. Cylindrical geometry may be used in lieu of spherical coordinates to describe a spherical problem. In this section, we demonstrate the use of R - Z geometry to preserve a 1-D spherical solution.

We use the MMS with

$$\psi_{\text{MMS}}(r, z) = \rho = \sqrt{r^2 + z^2}. \quad (54)$$

This solution is linear in the 1-D spherical coordinate ρ . We solve this for $p = \{1, 2, 4\}$, using S_N level symmetric angular quadrature with $N = \{4, 6, 8, 10, 12\}$, on a 1st- and 2nd-order mesh. The problem has physical parameters $\sigma_t = 5.0$ and $\sigma_a = 2.0$. Figures 8 - 10 show each finite element order p for select angular quadrature solutions.

We see from Figures 8 - 10 that increasing the angular quadrature order does qualitatively reduce the general asymmetry of the solution. Increasing the finite element order, however, reduces the asymmetry significantly more. Figure 12 compares $p = \{1, 2, 4\}$ for S_8 level-symmetric angular quadrature. We notice that the solution around $\rho = 0$ persistently has the largest asymmetries. We note that this mesh is made up entirely of quadrilaterals, even the inner-most radial zones.

Although the manufactured solution (Eq. 54) is not overly complicated, a steep gradient appears in the MMS source term near $(r, z) = (0, 0)$. We look at each term of the transport equation using the manufactured solution in Figure 17. The shape of the source term $S_0/(2\pi)$ is complicated near the origin. In practice, the source term is approximated by the finite element shape function using the analytic values for the nodes. So although the source is exact at the node points, the shape function does not capture the analytic shape of the source term necessary to achieve the axisymmetry

we desire.

We also investigated the symmetry preservation by performing sequential mesh refinements for $p = 1$. Figures 18 and 19 show the first several mesh refinement steps.

We also investigated the symmetry preservation by performing sequential mesh refinements for $p = 4$. Figures 20 and 21 show the first several mesh refinement steps.

1.6 Other

1.7 Material Discontinuity Stress Test

We adapted this problem from Palmer [?] and solved it without DSA in Woods et al. [?]. There are five different material regions described in Table 1 and Figure 22.

Table 1: Material discontinuity stress test with MIP DSA material properties.

Material Region	$\sigma_t \text{ cm}^{-1}$	$\sigma_s \text{ cm}^{-1}$	$S_0 \text{ cm}^{-2} \text{ s}^{-1}$
Source	1.0	1.0	1.0
Very thin absorber	0.0001	0.0	0.0
Thick absorber	10.0	0.0	0.0
Very thick absorber	100.0	0.0	0.0
Very thick scatterer	1000.0	1000.0	0.0

This problem has opacities that range several orders of magnitude, resulting in strong material discontinuities. We also introduce anisotropic incident intensities into the scattering region by preferentially attenuating intensities that are not perpendicular to the thick absorber. We expect some degradation in the DSA in problems with strong material discontinuities [?]. We also expect boundary layers to form from the anisotropic incident intensities [?]. The solution is shown in Figure 23.

1.8 Reflecting Boundary Conditions

To incorporate reflecting boundary conditions, we will “guess” the incident angular fluxes, update them with outgoing angular fluxes from the previous iteration, and adapt a convergence criterion for those fluxes. Along the z-axis, the reflection for direction $\Omega = (\mu, \eta, \xi)$ is $\Omega_R = (-\mu, \eta, \xi)$.

1.9 Reflecting Boundary Conditions

This may not warrant an entire subsection.

Reflecting boundaries are dependent upon the direction of the outgoing angular flux, Ω_m . The reflected incident direction is

$$\Omega^R = \Omega_m - 2(\Omega_m \cdot \hat{n})\hat{n} \quad (55)$$

where Ω_m is the outgoing direction and \hat{n} is the unit normal vector on the boundary (pointing outward). We apply a Dirichlet boundary condition for the angular flux in the reflected direction,

$$\psi^b(\mathbf{r}, \Omega^R) = \psi_m \quad (56)$$

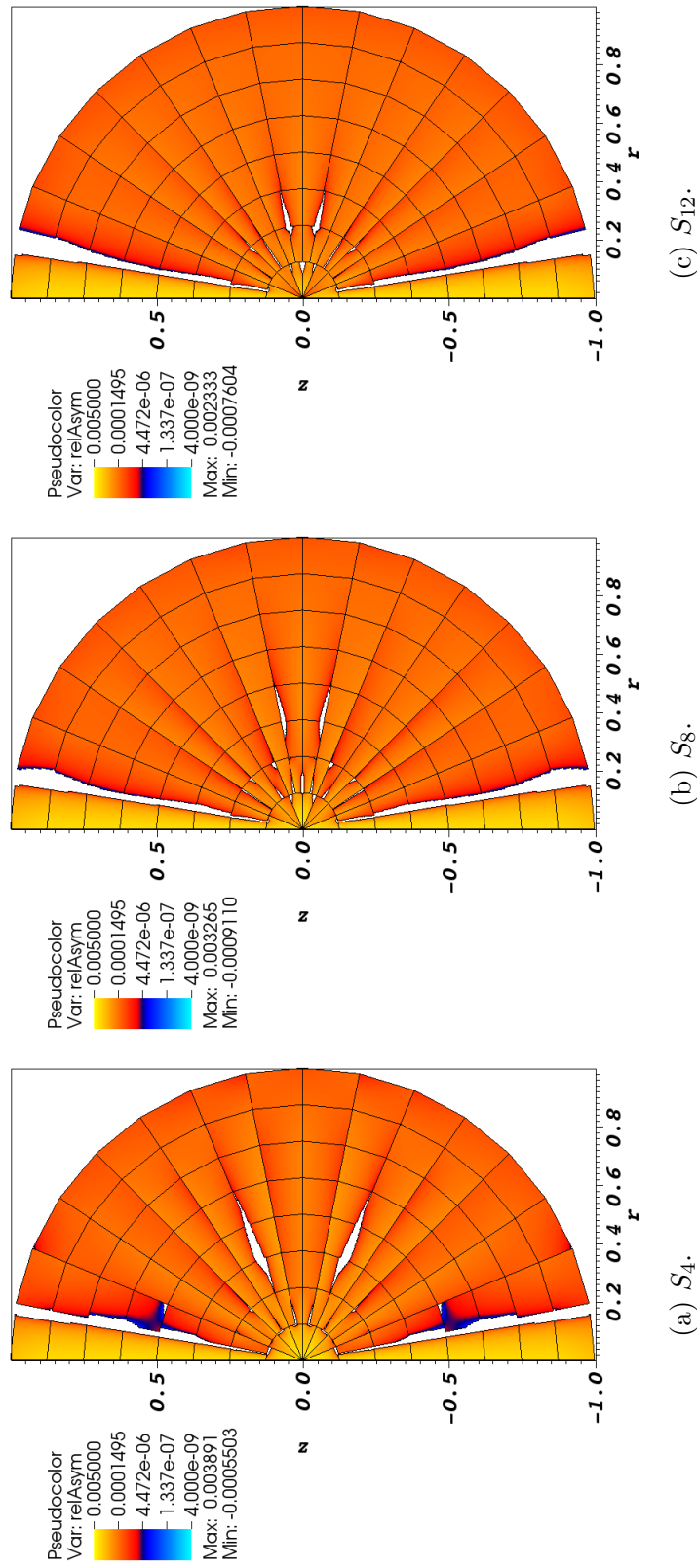


Figure 8: Relative asymmetry for 1st-order finite elements on a 1st-order mesh for given order of level-symmetric angular quadrature.

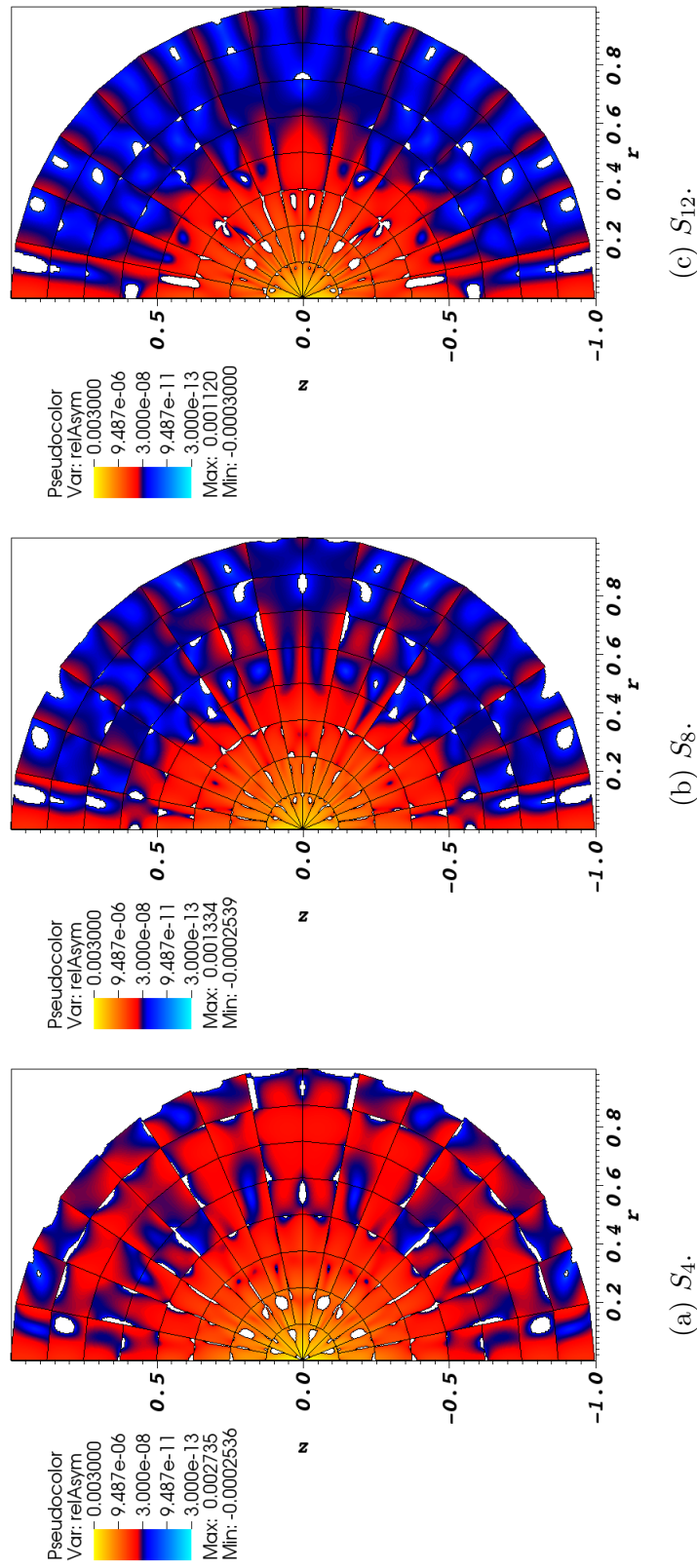


Figure 9: Relative asymmetry for 2st-order finite elements on a 1st-order mesh for given order of level-symmetric angular quadrature.

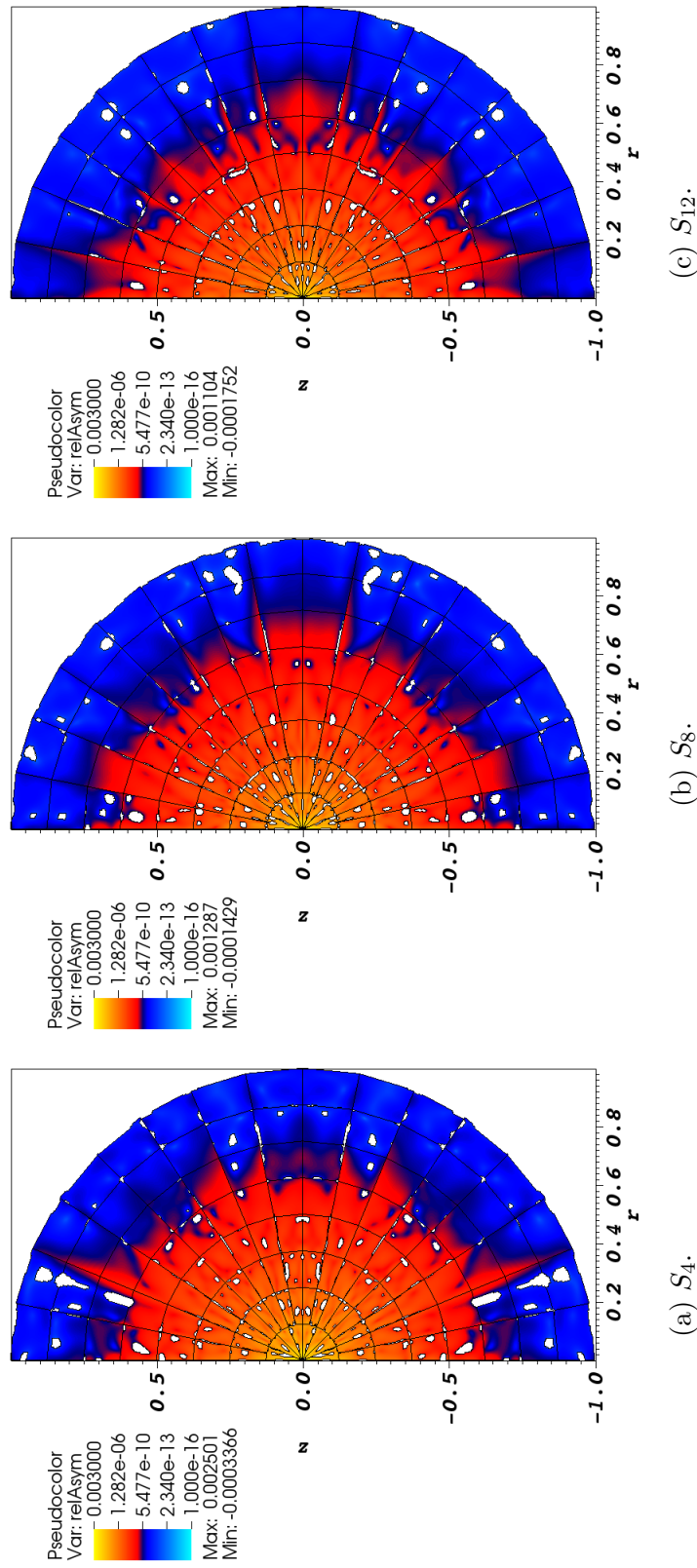


Figure 10: Relative asymmetry for 4st-order finite elements on a 1st-order mesh for given order of level-symmetric angular quadrature.

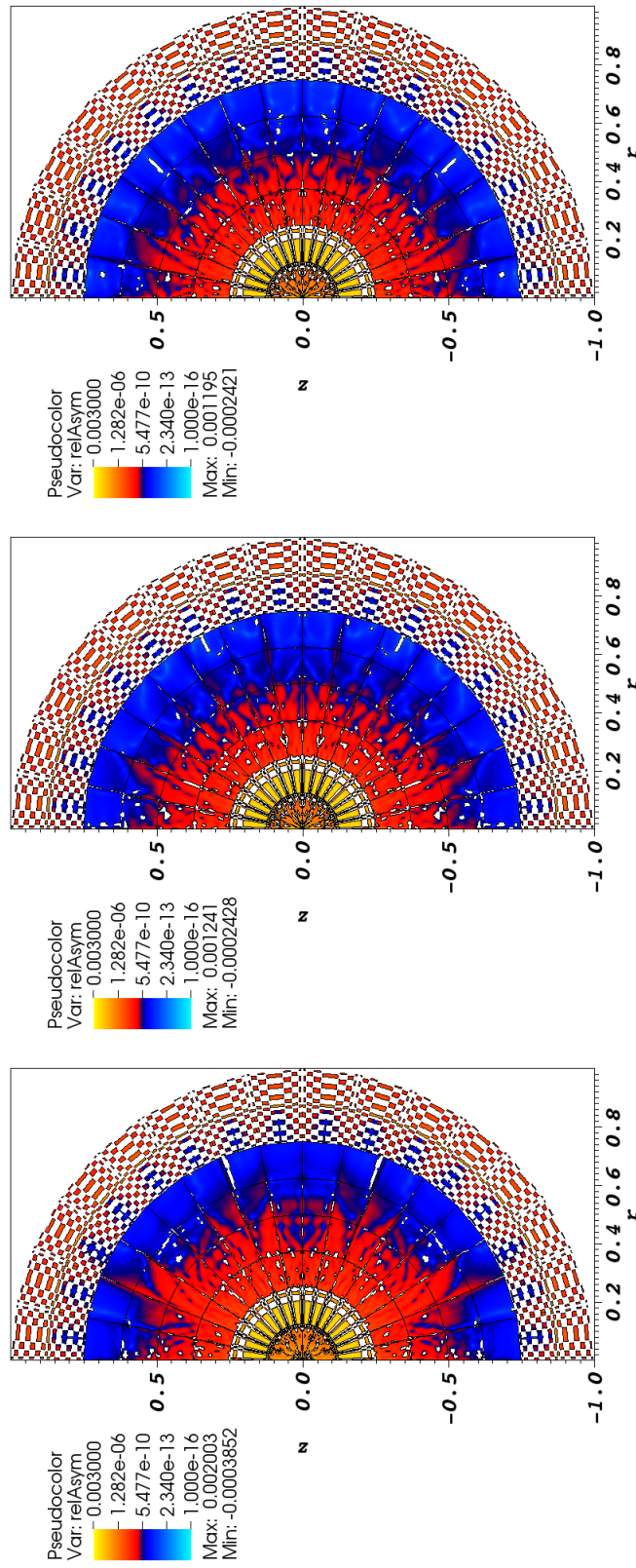


Figure 11: Relative asymmetry for 8st-order finite elements on a 1st-order mesh for given order of level-symmetric angular quadrature.

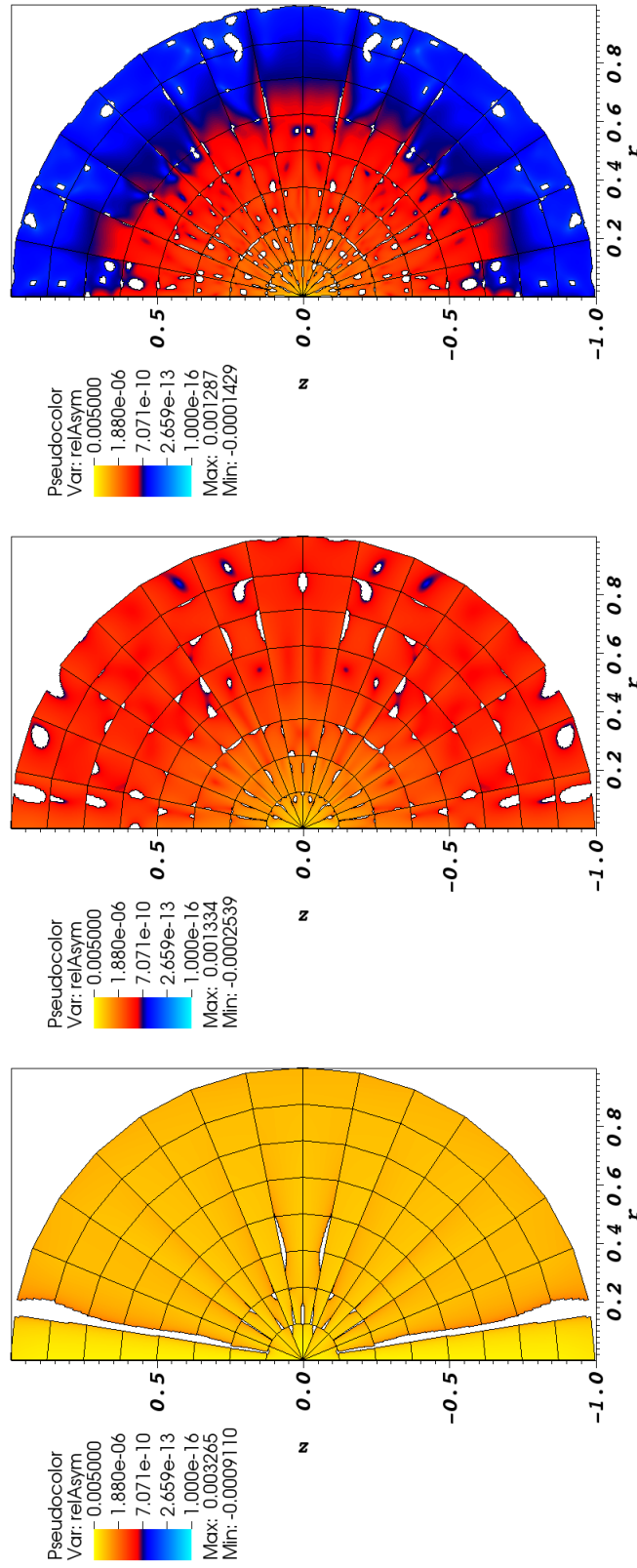


Figure 12: Relative asymmetry for $p = \{1, 2, 4\}$ finite elements on a 1st-order mesh for S_8 level-symmetric angular quadrature.

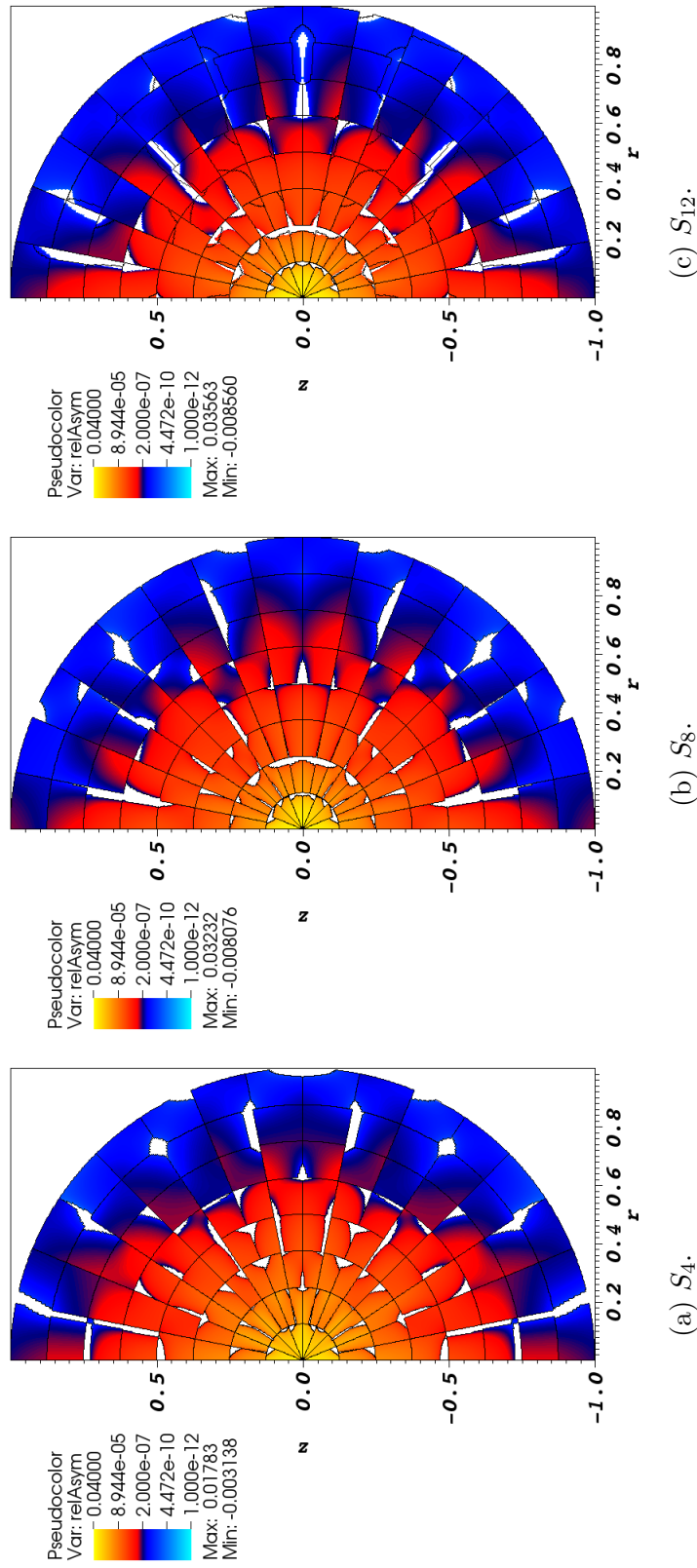


Figure 13: Relative asymmetry for 1st-order finite elements on a 2nd-order mesh for given order of level-symmetric angular quadrature.

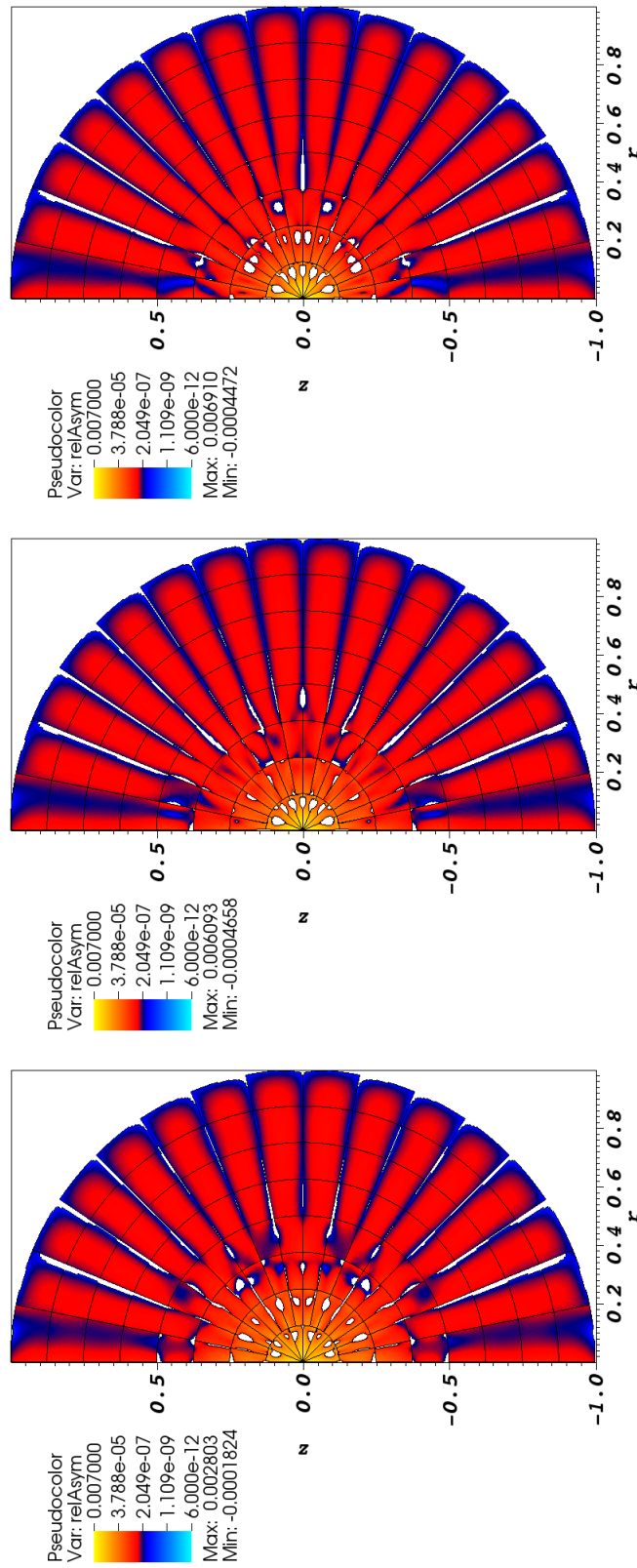


Figure 14: Relative asymmetry for 2nd-order finite elements on a 2nd-order mesh for given order of level-symmetric angular quadrature.

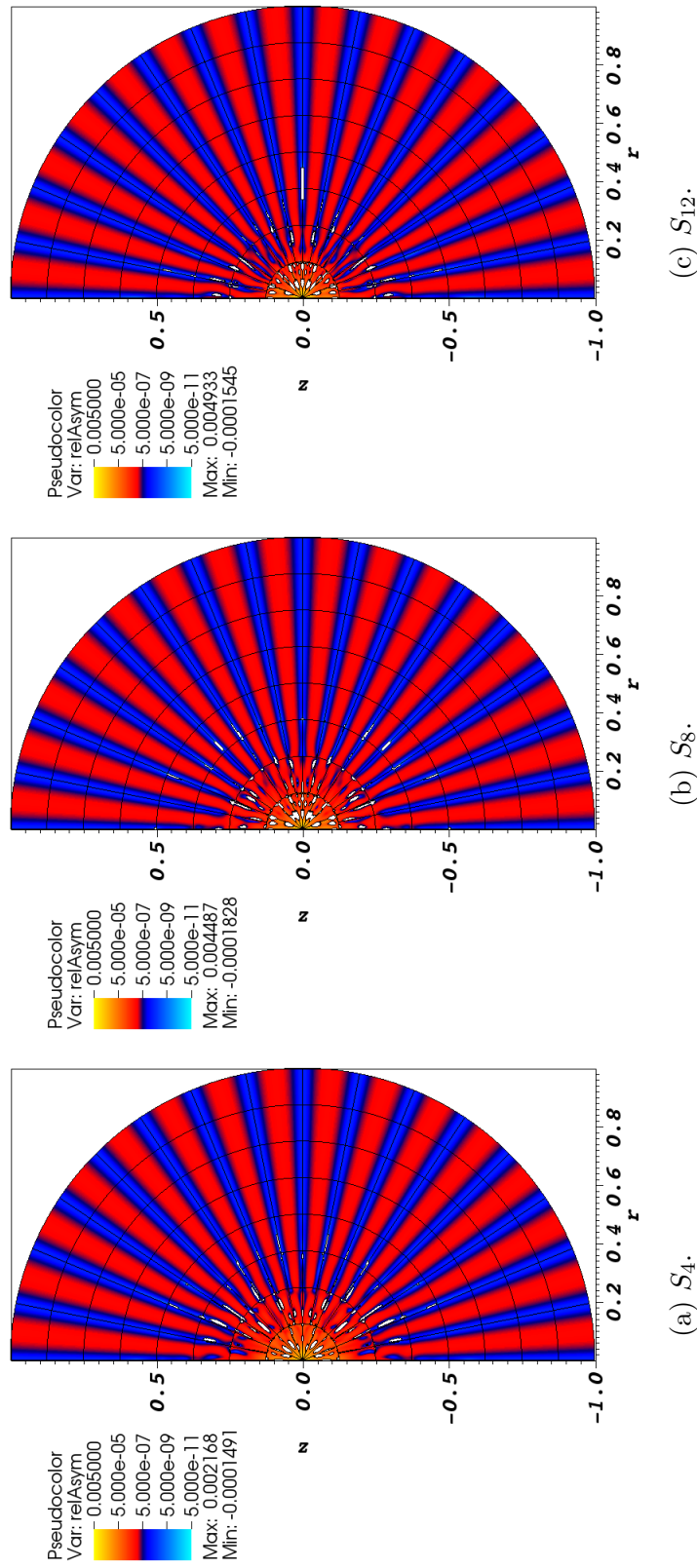


Figure 15: Relative asymmetry for 4th-order finite elements on a 2nd-order mesh for given order of level-symmetric angular quadrature.

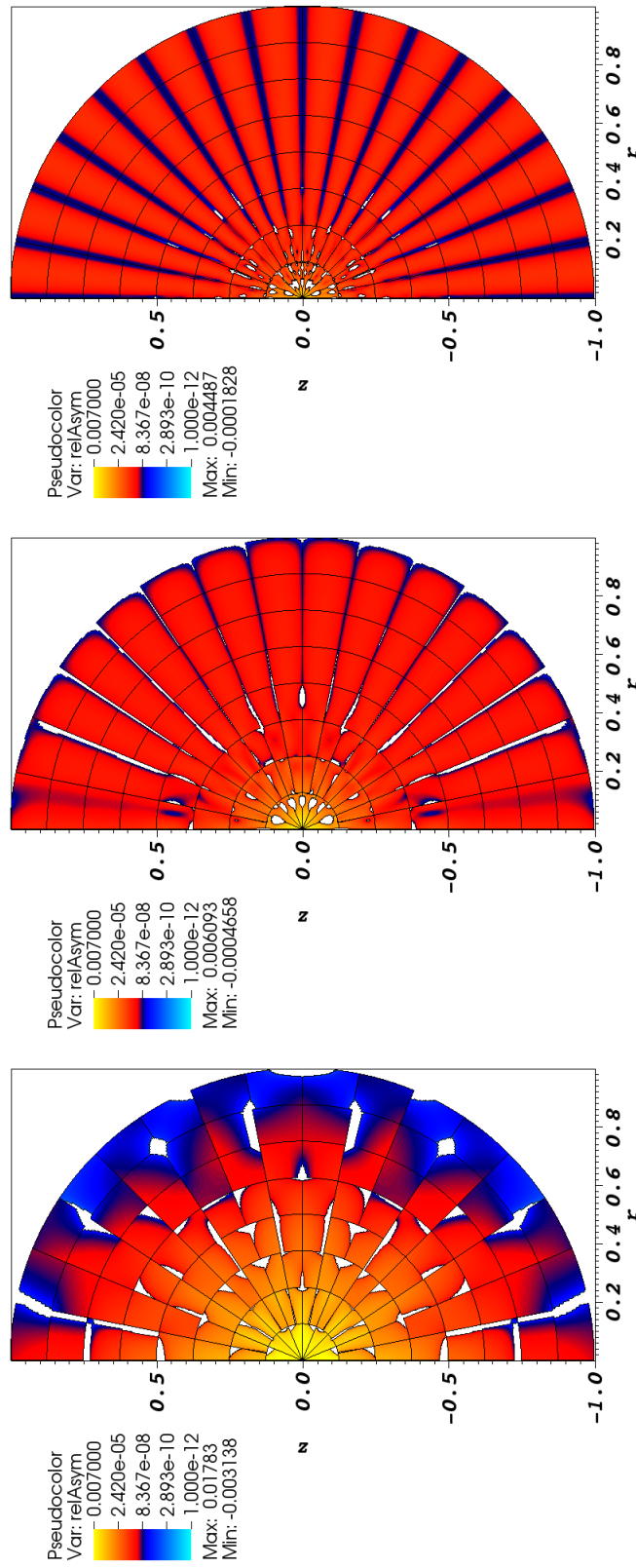


Figure 16: Relative asymmetry for $p = \{1, 2, 4\}$ finite elements on a 2nd-order mesh for S_8 level-symmetric angular quadrature.

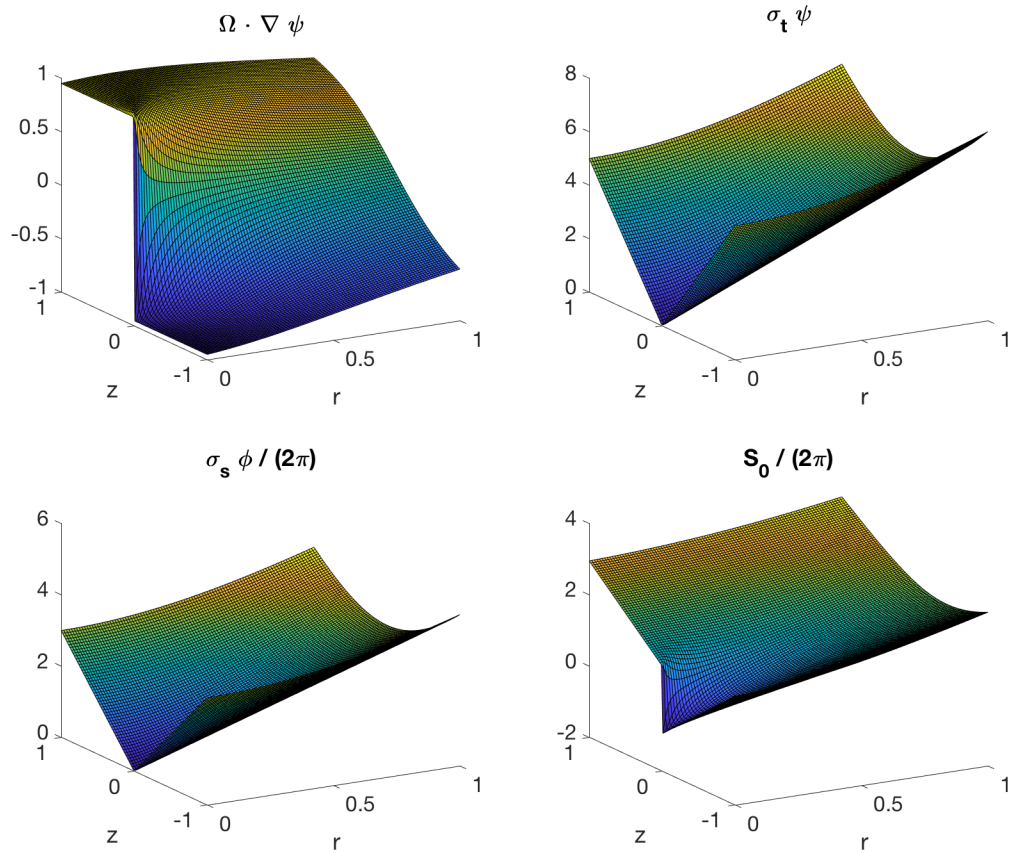


Figure 17: Analytic representation of each term of the transport equation using the manufactured solution, Equation 54, for $(\mu, \xi) = (0.21821789023599239, 0.95118973121134187)$. The complicated shapes of the streaming and source terms are typical of the other Ω directions.

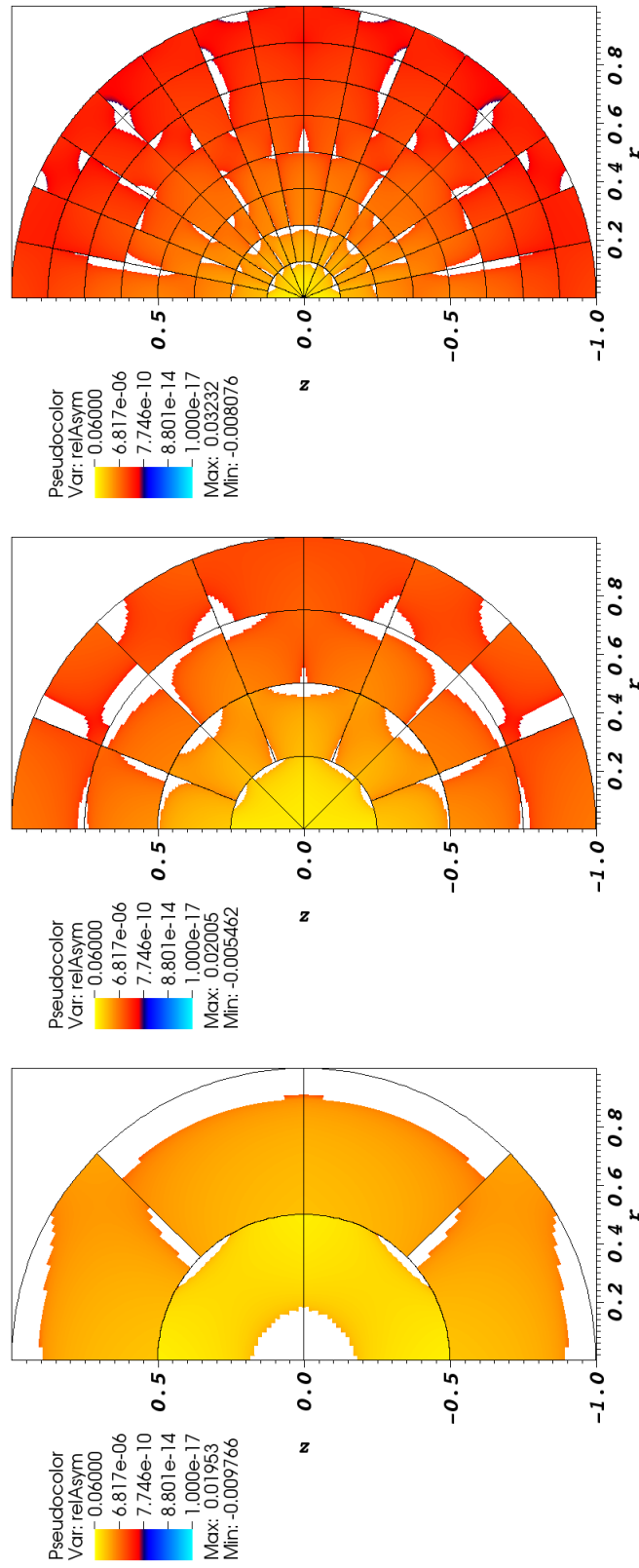


Figure 18: Relative asymmetry for $p = 1$ finite elements on a 2nd-order mesh for S_8 level-symmetric angular quadrature.

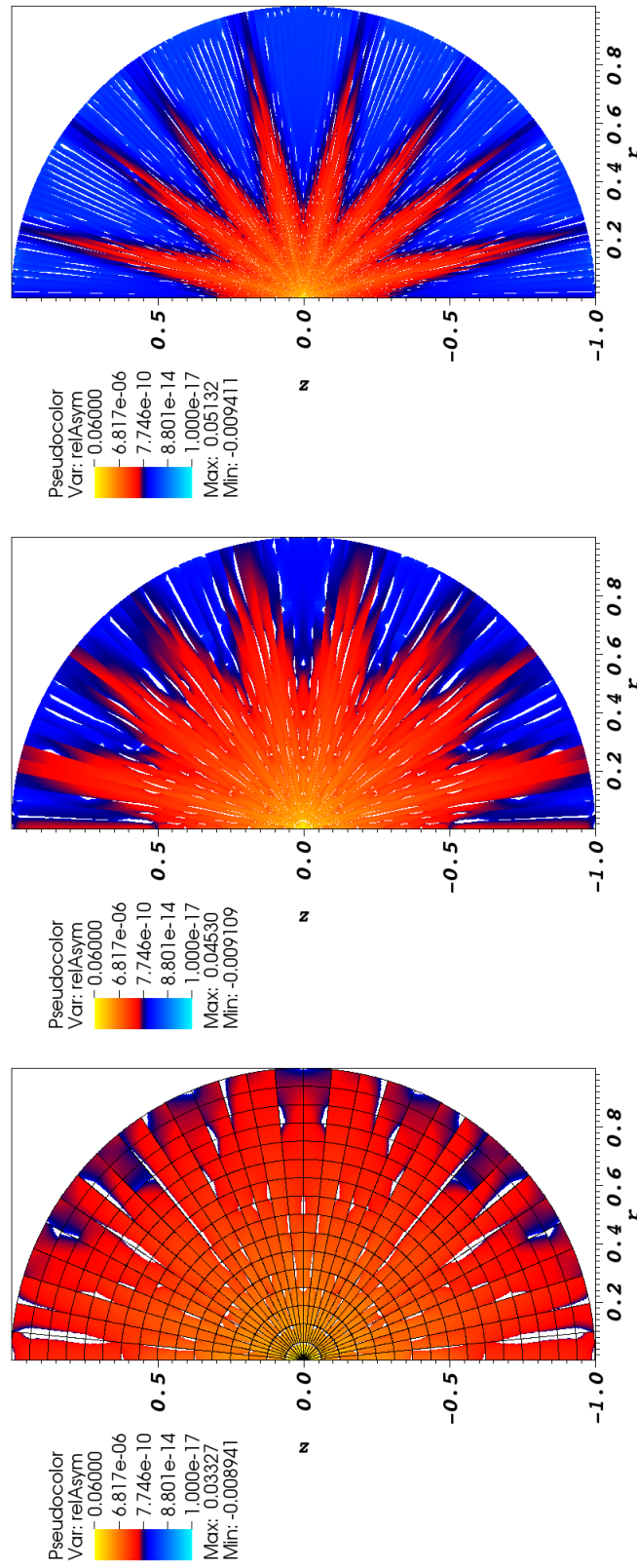


Figure 19: Relative asymmetry for $p=1$ finite elements on a 2^{nd} -order mesh for S_8 level-symmetric angular quadrature; mesh overlay may be removed for clarity.

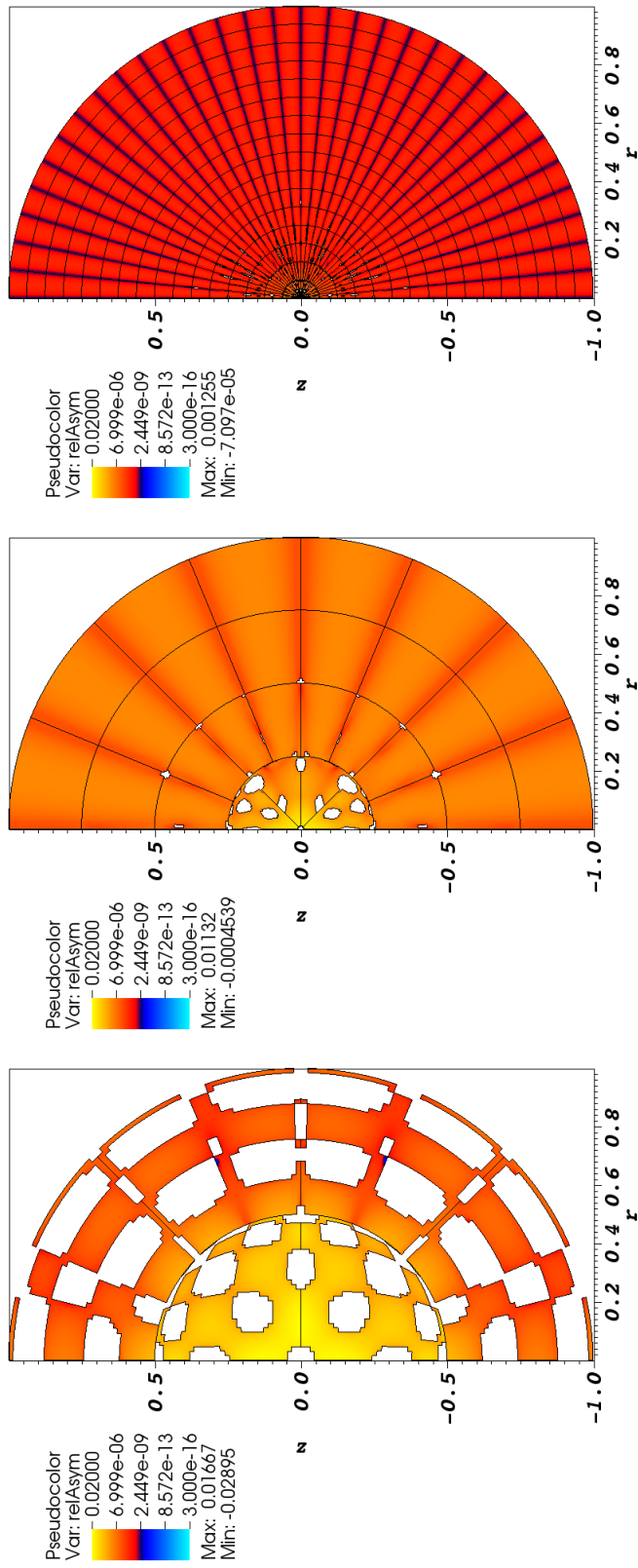


Figure 20: Relative asymmetry for $p = 4$ finite elements on a 2nd-order mesh for S_8 level-symmetric angular quadrature.

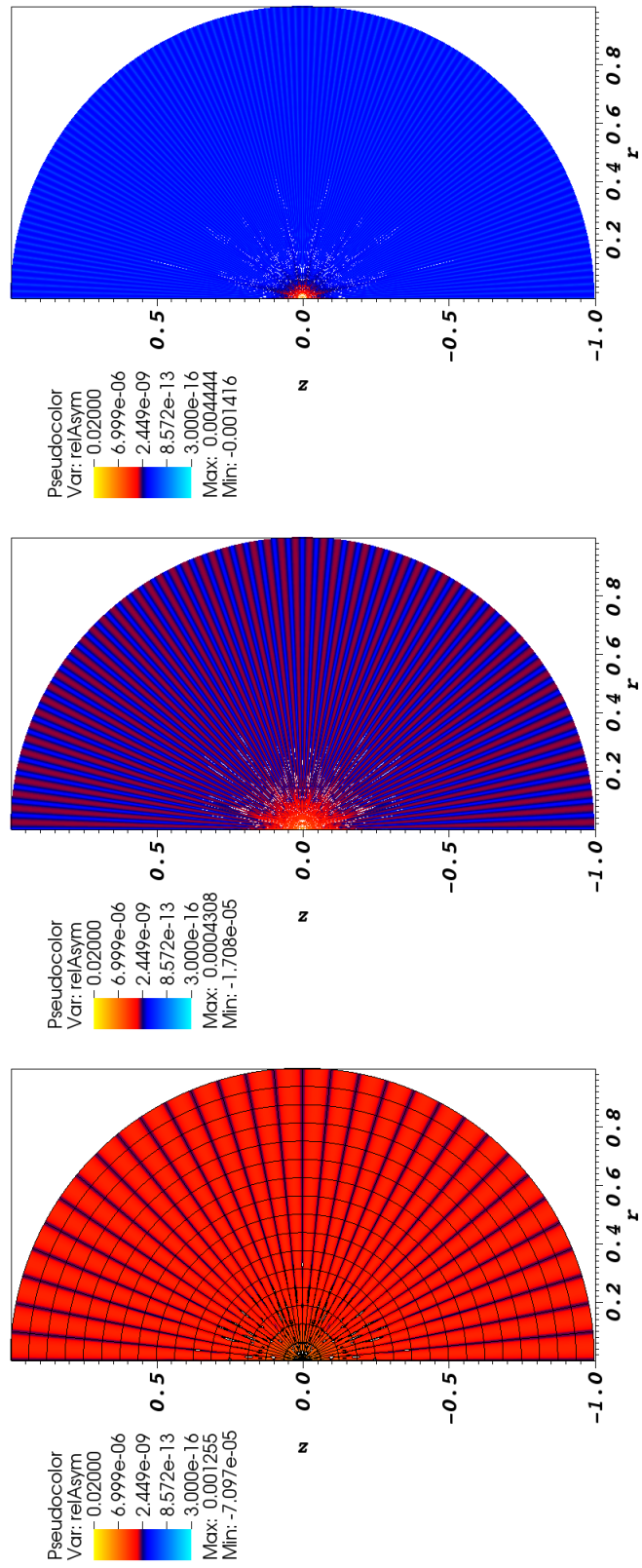


Figure 21: Relative asymmetry for $p = 4$ finite elements on a 2nd-order mesh for S_8 level-symmetric angular quadrature; mesh overlay may be removed for clarity.

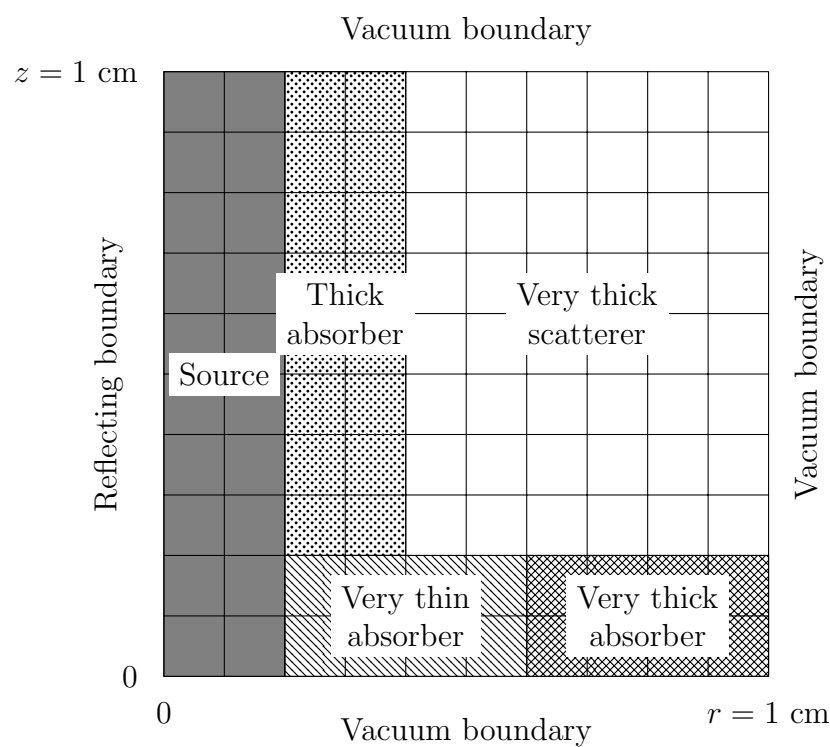
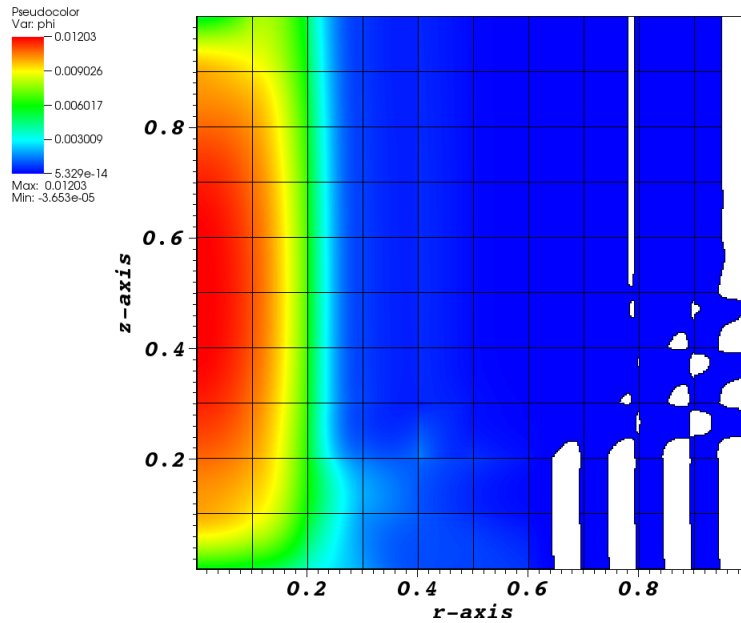
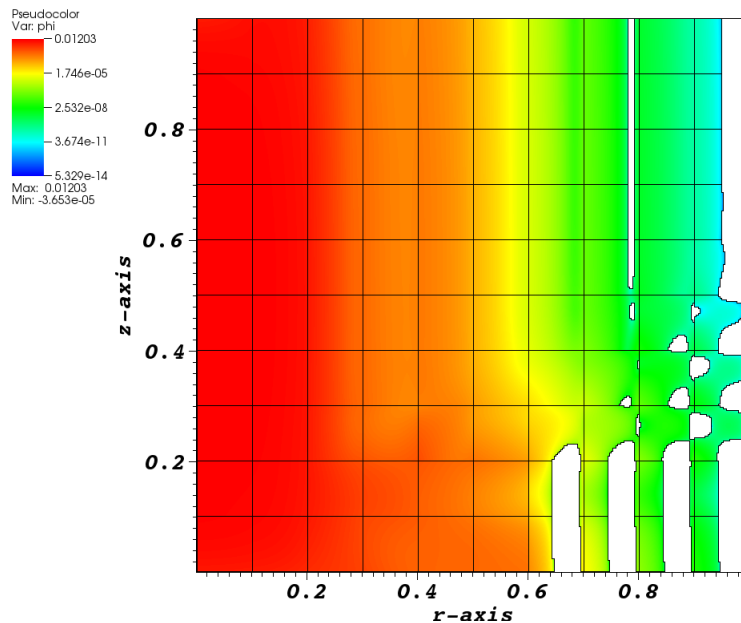


Figure 22: Material discontinuity stress test with MIP DSA problem geometry; materials defined in Table 1.



(a) Scalar flux.



(b) Log of scalar flux.

Figure 23: Solution to multi-material stress test. White regions indicate negative scalar fluxes. This was solved without DSA and was only allowed 10,000 source iterations to complete.